IEEE Access
Multidisciplinary | Rapid Review | Open Access Journal

Received 10 May 2022, accepted 23 June 2022, date of publication 28 June 2022, date of current version 5 July 2022.

Digital Object Identifier 10.1109/ACCESS.2022.3186888

RESEARCH ARTICLE

A Binary Classification Study of Alzheimer's Disease Based on a Novel Subclass Weighted Logistic Regression Method

JINHUA SHENG[1,2], (Senior Member, IEEE), SHUAI WU[1,2], QIAO ZHANG[3,4], ZHONGJIN LI[1,2], AND HE HUANG[1,2]

[1]College of Computer Science and Technology, Hangzhou Dianzi University, Hangzhou, Zhejiang 310018, China
[2]Key Laboratory of Intelligent Image Analysis for Sensory and Cognitive Health, Ministry of Industry and Information Technology of China, Hangzhou, Zhejiang 310018, China
[3]Beijing Hospital, Beijing 100730, China
[4]Institute of Geriatric Medicine, Chinese Academy of Medical Sciences, Beijing 100730, China

Corresponding author: Jinhua Sheng (j.sheng@ieee.org)

This work was supported in part by the National Natural Science Foundation of China under Grant 61871168; and in part by the Alzheimer's Disease Neuroimaging Initiative (ADNI), National Institutes of Health, USA, under Grant U01 AG024904.

ABSTRACT Based on proposed joint human connectome project multi-modal parcellation (JHCPMMP), the study on the binary classification of Alzheimer's disease was conducted. We tried to build a novel classification model, which can be interpretative and have the ability to deal with the complexity and individual differences of brain networks. The subclass weighted logistic regression (SWLR) based on logistic regression was proposed in this paper. We conducted five groups of experiments, in which the accuracy of HC vs. AD was 95.8%, HC vs. EMCI was 91.6%, HC vs. LMCI was 93.7%, EMCI vs. LMCI was 89.5%, and LMCI vs. AD was 91.6%. In addition, we conducted a follow-up analysis of the coefficient matrix and found that the distribution of core deterioration brain regions in different stages is different in the development of Alzheimer's disease. We located these brain regions in two-dimensional images and found that they generally show a trend of continuous counterclockwise migration.

INDEX TERMS Alzheimer's disease, human connectome project (HCP), multi-modal parcellation (MMP), mild cognitive impairment (MCI), subclass-weighting.

I. INTRODUCTION

Alzheimer's disease (AD) is a neurodegenerative disease. It destroys brain cells, leads to abnormalities in memory, cognition, thinking and behavior, and seriously affects people's work and life until the body loses its function. Dementia mainly occurs in people over the age of 60. The extension of life expectancy leads to a rapid increase in the number of patients with dementia [1]. According to the world Alzheimer's disease report [2], about 50 million people were affected by the disease in 2018, which is expected to triple by 2050. In addition, Alzheimer's disease has irreversible characteristics, so how to confirm the stage of patients and treat them is very important to alleviate the development of the disease.

Mild cognitive impairment (MCI) is a widely used term that describes the intermediate stage from normal cognitive function to dementia. Patients with mild cognitive impairment have a high rate of developing dementia in a relatively short time, even among subjects who returned to normal cognition, the incidence of subsequent mild cognitive impairment or dementia was higher than those who had never experienced mild cognitive impairment [3]. The recent extensions of ADNI (ADNI go, ADNI 2) have introduced the distinction of MCI into early and late MCI. Late MCI (LMCI) refers to the original definition (performance of 1.5 SD below the normative mean), whereas in early MCI (EMCI), impairment is defined as performance between 1.0 SD and 1.5 SD below the normative mean on a standard test [4].

The associate editor coordinating the review of this manuscript and approving it for publication was Sunil Karamchandani.

The diagnosis of Alzheimer's disease by brain imaging technology is one of the commonly used methods in medicine. Structural MRI is the most widely used brain imaging method in AD research. FDG PET is the most characteristic functional brain imaging method in AD research, DTI has been used to study the integrity and connectivity of white matter in patients with dementia and high-risk patients, single photon emission computed tomography (SPECT) uses a radioactive tracer to track brain perfusion for dementia, which is very similar to PET scanning of glucose metabolism in clinical diagnosis [5]. Functional magnetic resonance imaging (fMRI) has been proved to be immeasurable value in identifying the neural structures of human behavior and cognition [6], [7], and the main principle is blood oxygenation level dependent [8]. fMRI is divided into task fMRI and resting state fMRI. Resting state fMRI captures the changes in blood oxygenation levels of subjects in the rest state task fMRI captures the changes in blood oxygenation levels of subjects in the task state. In fact, the internal network extracted from task scanning is very similar to that extracted from static state scanning. At present, some studies [9]–[12] have used task scanning for internal connection analysis when there is no static state data.

The human connectome project (HCP) proposes a multimodal parcellation (MMP) of human cerebral cortex. HCPMMP is an adaptive brain zoning method with four modes, including cortical thickness, myelin map, task fMRI and resting state fMRI. Under the conditions of zoning specification and coordinate unified space, it can divide the left and right brains of different people into 180 regions [13]. Joint-HCPMMP is a new data preprocessing method based on HCPMMP data preprocessing method proposed by us [14], which can appropriately reduce the data requirements of HCP preprocessing framework. Our experimental data are obtained based on Joint-HCPMMP method.

At present, machine learning and deep learning have been widely used in the classification of neuroimaging data. In machine learning, Gosztolya *et al.* [15] by automatically extracting acoustic markers from subjects' self-speaking utterances and using linear SVM for classification,and accuracies of 80%, 86%, and 80% have been achieved for CN vs. MCI, CN vs. mild AD (mAD), MCI vs. mAD. Peng *et al.* [16] selected MRI and genetic features, and used multi-kernel learning of support vector machine. Accuracy of CN vs. AD, and CN vs. MCI are 96.1% and 80.3%, respectively. In deep learning, Wang *et al.* [17] developed an ensemble of 3D densely connected CNNs (3D-DenseNets), which maximizes the information flow from one layer to next layer and accuracies of 93.61%, 98.42%, and 98.83% have been achieved for AD vs. stable MCI (sMCI), CN vs. sMCI, CN vs. AD. Spasov *et al.* [18] used deep CNN for extracting the descriptive features from structural MRI (sMRI) T1 based on 3D separable and grouped convolutions. CNN was used for classification with accuracies of 100%, and 92.5% for CN vs. AD, sMCI vs. progressive MCI (pMCI).

Although there are many classification studies on Alzheimer's disease, we have noticed that most studies focus on the three stages of HC, MCI, and AD. Therefore, in this experiment, four stages of HC, EMCI, LMCI and AD were selected for classification. On this basis, we hope that our research is not limited to the index of accuracy. An excellent model should enable us to obtain useful information. In this way, the finer the division of disease stages, the better we can understand the development of disease through the model. We note that the logistic regression algorithm has good interpretability. However, the brain network constructed in this experiment is very complex, and there are still interference factors such as individual differences. Therefore, the traditional logistic regression cannot show satisfactory results in the face of this task. Therefore, we proposed a subclass weighted logistic regression (SWLR) algorithm on the basis of traditional logistic regression. Firstly, we select the appropriate clustering algorithm to divide the samples into different subclasses. Then, on the basis of global coefficients, we construct subclass coefficients for each subclass to realize the weighting of different subclasses. Finally, we obtain the optimal accuracy through continuous iterative optimization.

II. MATERIALS AND METHODS

The experimental data in this paper are from Alzheimer's disease neuroimaging Initiative (ADNI). ADNI is an open database for the world. Its main purpose is to predict, diagnose and treat Alzheimer's disease, and provide reliable medical imaging data and clinical data for Alzheimer's researchers all over the world. The experimental data in this paper include HC, EMCI, LMCI and AD, with 24 subjects in each group, a total of 96 people. The demographic information of subjects is shown in Table 1. All methods were carried out in accordance with relevant guidelines and regulations. All experimental protocols were approved by the institutional review board (IRB) at Hangzhou Dianzi University (IRB-2020001).

A. DATA PREPROCESSING

HCP preprocessing pipeline was used to process MRI structure data, including denoising, standardization, distortion correction and spatial transformation, and align and register brain data into CIFTI space. Based on surface analysis, CIFTI defines 91,282 standard gray coordinates, including 26,298 subcortical voxels in 2mm MNI space and 32,492 surface vertices in each hemisphere. HCPMMP obtains 180 brain regions in each hemisphere through multimodal segmentation on these gray coordinates. After the structural pipeline was completed, the functional pipeline was carried out, including removing the spatial distortion in the functional magnetic resonance imaging data, rearranging the volume to compensate for the movement of the subject, registering the fMRI data on the structure, reducing the bias field, normalizing the 4D image, and finally mapping these time series from the volume to the CIFTI gray coordinate space. After the above

TABLE 1. Information of acquired ADNI subjects.

HC	Sex	Age	EMCI	Sex	Age	LMCI	Sex	Age	AD	Sex	Age
033_S_4176	M	90.5	137_S_4536	F	83.6	941_S_4187	M	67.8	136_S_4993	F	71.9
116_S_4453	M	72	137_S_4351	F	73.8	141_S_1378	F	72.1	130_S_5231	F	74.4
941_S_6094	F	69.6	137_S_4299	F	82.9	141_S_1052	F	80.7	130_S_5059	M	72.8
168_S_6131	F	68.3	114_S_2392	F	70.6	068_S_4061	F	70.5	130_S_4990	F	75.7
168_S_6085	F	55.8	094_S_2238	M	75.6	068_S_0802	F	91.8	130_S_4984	F	73.2
168_S_6098	M	63.4	094_S_2201	F	70.5	067_S_4782	M	77.1	130_S_4971	M	77.1
137_S_4482	F	83	082_S_2121	F	75.2	067_S_4767	F	71.4	130_S_4730	F	81.2
116_S_6119	F	67.1	068_S_4431	M	79.8	041_S_4510	F	72.1	130_S_4660	F	77.3
114_S_6063	F	74.3	068_S_4067	M	71.2	041_S_1418	M	91.6	130_S_4641	F	73.9
114_S_0416	F	87.2	068_S_2315	F	74.9	041_S_0679	M	74	130_S_4589	F	75.2
094_S_4649	M	71.2	068_S_2184	F	87.4	037_S_4214	M	79.6	100_S_5106	M	74.3
041_S_6192	F	83.3	067_S_4212	M	70.9	037_S_4030	F	74.7	053_S_5208	M	68.8
041_S_6159	M	76.3	067_S_4184	F	68.6	037_S_0377	M	91.3	053_S_5070	M	72.4
041_S_4200	F	76.4	067_S_4072	F	68.5	036_S_4715	F	62.2	019_S_5012	M	76.4
037_S_4028	F	70.7	067_S_2301	M	72.2	036_S_4538	F	84.5	019_S_4549	M	79.4
036_S_6189	F	69.6	041_S_4974	M	78.4	036_S_4430	M	85.9	019_S_4477	F	82.4
035_S_6160	M	60.7	041_S_4513	M	66.4	035_S_4414	F	66.4	019_S_4252	F	86.8
033_S_4177	M	91.4	037_S_4706	M	66.2	023_S_4115	M	73.9	018_S_5074	F	74.9
023_S_1190	F	87.4	014_S_2308	M	81.4	003_S_4354	M	81.3	018_S_4733	M	75.4
020_S_6185	M	82.7	012_S_4188	M	83.2	003_S_1122	F	87.2	018_S_4696	F	73.3
011_S_0021	F	84.9	011_S_4893	F	73.4	003_S_1074	F	95.9	013_S_5071	M	76.4
007_S_4387	F	82	011_S_4547	M	82.8	002_S_4654	F	80.5	006_S_4867	M	75.7
007_S_1222	F	84.4	007_S_4272	M	77.2	002_S_4229	M	72.4	006_S_4153	M	81.5
003_S_4288	F	78.4	002_S_4473	M	79.9	002_S_1155	M	68.2	002_S_5018	M	73.4

TABLE 2. Global cost efficiency of four groups of samples.

	HC	EMCI	LMCI	AD
GCE	0.329±0.040	0.323±0.037	0.326±0.045	0.319±0.035

steps, we obtained the segmentation of 360 brain regions and the corresponding signal sequence, and then we calculated the correlation between any two brain regions through the Pearson correlation coefficient to obtain the functional brain network. On this basis, we build a weighted network and a binary network, the key to building a binary network is to find an appropriate threshold. We use the proportion of strongest weights (PSW) algorithm to determine the threshold [19]. Specifically, we set a step size for PSW and continuously adjust the value of PSW through iteration to maximize the global cost efficiency (GCE) parameters in the brain connection matrix. In this algorithm, the PSW value is defined as the ratio of the number of reserved strong weights to the total number of weights. Through this process, we eliminate some edges with small weights to maintain significant connections between regions of interest (ROIs). The specific formula of the algorithm is as follows:

$$E = \frac{1}{n}\sum_{i\in N}\frac{\sum_{j\in N, j\neq i} d_{ij}^{-1}}{n-1} \tag{1}$$

$$\max_{psw}(GCE) = E - PSW \tag{2}$$

The average GCE values of the four groups of samples are shown in Table 2.

B. CONSTRUCTION OF FEATURE MATRIX

After the previous step, we obtained weighted networks and binary networks. The next step is to select the evaluation index of complex brain network and establish the characteristic matrix. For the evaluation method of complex brain network, the global evaluation index and the local evaluation index are representative. Seven brain network evaluation indexes were selected in the case of weighted network or binary network. They are: clustering coefficient (binary, weighted), degree (binary), efficiency (binary, weighted), eigenvector centrality (binary, weighted), assortativity (weighted), k-coreness centrality (binary) and strength (weighted). We can see that among the seven indexes, efficiency, eigenvetor centrality and clustering can be calculated based on both weighted network and binary network. We finally get 10 results with 10×360 features, which correspond to 180 brain regions of the left and right brain, according to these features. We establish a 48×3600 size feature matrix for each binary classification. The calculation process of global and local metric parameters of brain network is very complex. In this paper, we calculated all required parameters with the help of brain connectivity toolbox (https://sites.google.com/Site/bctnet/).

C. SUBCLASS WEIGHTED LOGISTIC REGRESSION

The idea of traditional logistic regression algorithm is to constantly adjust the weight coefficient corresponding to each feature, and establish a hyperplane according to the weight coefficient to distinguish the two types of samples, so as to minimize the value of loss function. However, as the samples become more and more complex and the feature dimension becomes higher and higher, the traditional logical regression can no longer meet the current needs. Therefore, we propose a new algorithm: subclass weighted logistic regression algorithm. The specific idea of SWLR algorithm is to use the training set data to do a logistic regression first, and find the best global coefficient matrix U on the training set, and build a subclass coefficient matrix for each subclass on the basis of U. finally, the prediction label of a sample is jointly determined by the global coefficient and subclass

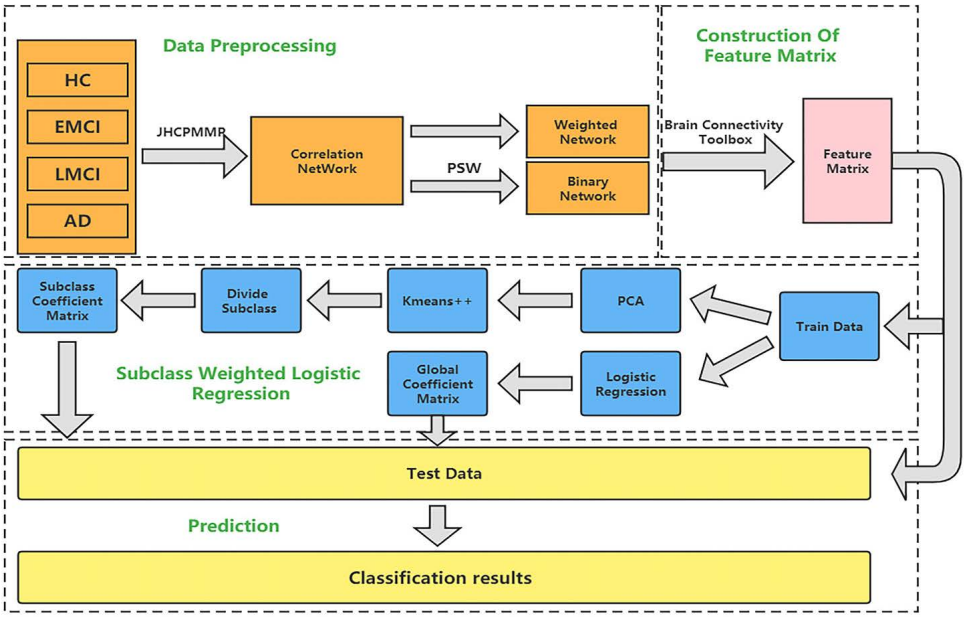

FIGURE 1. Subclass weighted logistic regression flow chart.

coefficient. In order to construct the subclass coefficient matrix, we will use k-means++ clustering for the feature matrix. Theoretically, sample with close Euclidean distance are more likely to have the same label. It is worth mentioning that when the number of features is particularly large, the clustering effect is often poor. Therefore, we use principal component analysis (PCA) technology to reduce the dimension of the characteristic matrix before clustering. The idea of PCA dimensionality reduction is to project the data from high-dimensional space to low-dimensional subspace through linear projection, and expect the variance of the projected data to be as large as possible, so as to retain the sample difference information of the original data to the greatest extent. Our goal is to minimize the loss function, so we use the gradient descent method for iterative optimization. In addition, in order to prevent over fitting, we have L2 regularized the global coefficients and subclass coefficients. The specific algorithm flow is shown in Figure 1. The formula of the algorithm is as follows:

$$z_i = x_i^T U + x_i^T V^{g_m} \tag{3}$$

where, z_i is Intermediate variable In the following formula, it is used to calculate the predicted value of the sample, x_i represents different sample U represents global coefficient, V represents subclass coefficient, g_m represents different subclasses, and m takes 1-6 in this experiment.

$$\pi\left(z_i\right) = \frac{1}{1+e^{-z_i}} \tag{4}$$

$$J(U,V) = -\frac{1}{n}\sum_{i=1}^{n}\left\{y_i \log\left(\pi\left(z_i\right)\right) + \left(1-y_i\right)\log\left(1-\pi\left(z_i\right)\right)\right\} + \gamma_1 \|U\|_2^2 + \sum_{m=1}^{6}\gamma_{m+1}\left\|V^{g_m}\right\|_2^2 \tag{5}$$

where, $\pi(z_i)$ is the predicted value, $J(U, V)$ is the loss function, y_i is the sample label.

Since there are two variables U and V in the objective function J, we choose to fix one variable to iteratively optimize the other variable until J converges. Specifically, we don't consider V at first, but only solve U:

$$\begin{aligned}\frac{\partial J}{\partial U_j} &= -\frac{1}{n}\sum_{i=1}^{n}\left\{y_i * \frac{1}{\pi\left(z_i\right)} * \frac{1}{\left(1+e^{-z_i}\right)^2} * \left(-e^{-z_i}\right)\right\} \\ &\quad -\frac{1}{n}\sum_{i=1}^{n}\left\{\left(1-y_i\right) * \frac{-1}{1-\pi\left(z_i\right)} * \frac{-1}{\left(1+e^{-z_i}\right)^2} * \left(-e^{-z_i}\right)\right\} \\ &\quad + \frac{\gamma_1}{2}U_j\end{aligned} \tag{6}$$

where, U_j represents the coefficients corresponding to different characteristics. According to Equation (6), we finally get that the partial derivative of j over U_j is:

$$\frac{\partial J}{\partial U_j} = -\frac{1}{n}\sum_{i=1}^{n}\left\{x_i\left(y_i - \frac{1}{1+e^{-z_i}}\right)\right\} + \frac{\gamma_1}{2}U_j \tag{7}$$

Then we update U_j:

$$U_j := U_j - \alpha\frac{\partial J}{\partial U_j} \tag{8}$$

After continuous iteration, we obtain an optimal global coefficient matrix U, and then we solve V of different

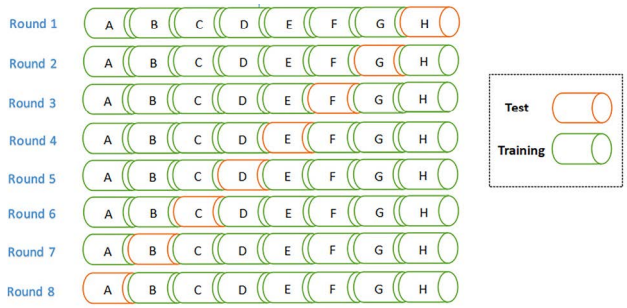

FIGURE 2. Illustration of 8-fold cross-validation.

subclasses on the basis of U, V_j represents the coefficient corresponding to different characteristics:

$$\frac{\partial J}{\partial V_j^{g_m}} = -\frac{1}{n}\sum_{i=1}^{n}\left\{y_i * \frac{1}{\pi(z_i)} * \frac{1}{\left(1+e^{-z_i}\right)^2} * \left(-e^{-z_i}\right)\right\} - \frac{1}{n}\sum_{i=1}^{n}\left\{(1-y_i) * \frac{-1}{1-\pi(z_i)} * \frac{-1}{\left(1+e^{-z_i}\right)^2} * \left(-e^{-z_i}\right)\right\} + \frac{\gamma_{m+1}}{2}V_j^{g_m} \quad (9)$$

After calculation, we finally get that the partial derivative of J over V_j is

$$\frac{\partial J}{\partial V_j^{g_m}} = -\frac{1}{n}\sum_{i=1}^{n}\left\{x_i\left(y_i - \frac{1}{1-e^{-z_i}}\right)\right\} + \frac{\gamma_{m+1}}{2}V_j^{g_m} \quad (10)$$

Then we update V_j:

$$V_j^{g_m} := V_j^{g_m} - \alpha\frac{\partial J}{\partial V_j^{g_m}} \quad (11)$$

After continuous iteration, we get the optimal subclass coefficient matrix V of different subclasses, and the predicted value of a sample can be calculated by Equation (3) and Equation (4).

III. RESULTS

We used subclass weighted logistic regression to classify the samples to test the effect of the model. The experiment was divided into HC vs. EMCI, HC vs. LMCI, HC vs. AD, EMCI vs. LMCI, LMCI vs. AD groups, with 48 samples in each group. Due to the small sample size, we adopted the 8-fold cross-validation technique shown in Figure 2. Specifically, we divide the 48 samples from each group into 8 subsets with 6 samples in each subset. We then used 7 of the 8 subsets for sequential training and the remaining one for testing, examining the effectiveness of the model by averaging the results of 8 cross-validations.

Let TP, TN, FP, and FN represent true positives, true negatives, false positives, and false negatives, respectively. We considered three indicators in total, namely Accuracy (ACC), Sensitivity (SEN), and Specificity (SPEC). They are calculated as follows: Accuracy = (TP + TN)/(TP + TN + FP + FN), Sensitivity = TP/(TP + FN), Specificity = TN/(TN + FP). Firstly, according to these indicators, we compare the performance of SWLR and different machine learning classifiers on our dataset. The results are shown in Table 3 it can be seen that our proposed SWLR method has achieved the highest accuracy in five groups, and the performance of traditional logistic regression on our data set is not ideal. Taking the accuracy rate as an example, the overall level is maintained at about 85%, while SWLR compared to LR has been greatly improved, of which the HC vs. AD group increased by 8.3%, the HC vs. EMCI group increased by 10.4%, the HC vs. LMCI group increased by 8.3%, the EMCI vs. LMCI group increased by 6.3%, the LMCI vs. AD group increased by 8.4%, and the five groups The accuracy was improved by an average of 8.34%. From the two aspects of SEN and SPEC, we find that there are obvious differences between LR and SWLR. The values of spec and Sen of LR algorithm are very different, one is very high and the other is very low, which seems to indicate that LR algorithm will sacrifice one of the positive and negative classes in order to ensure the overall prediction ability of the model this problem has been well solved in SWLR.

In addition, we also compared the SWLR method with the latest research methods. The results are shown in Table 4 it can be seen that our algorithm has achieved the best accuracy in HC vs. EMCI and EMCI vs. LMCI, and the accuracy of the other three groups is also very close to the current highest accuracy, which shows that our algorithm is effective. Because logistic regression has the advantage of strong interpretability, while SWLR retains this interpretability, we conducted a follow-up analysis of the coefficient matrix U to further explore the pathological process of the brain. In the logistic regression, the coefficients in the coefficient matrix represent the contribution of a feature to the classification results. Therefore, we extracted all the coefficients in U, grouped and summed all the coefficients according to brain regions, so as to evaluate the comprehensive importance of a brain region the brain regions were then ranked from high to low. Since the distribution of left and right brain regions is the same, we take the right brain as an example for discussion. We found that the number of brain regions in the top rankings is continuous or close, which means that these brain regions that have more influence on the human brain are likely to be concentrated in a certain area of the brain. To prove this point, we used the connectome workbench (https://www.nitrc.org/projects/workbench/) to locate the location of the core-brain regions of HC vs. EMCI, EMCI vs. LMCI, and LMCI vs. AD, and draw pictures.

It is worth mentioning that the selection of the number of core brain regions is also critical. Too few or too many are not conducive to the highlighting of the regularity. In Figure 3(a), Figure 3(b), and Figure 3(c), we selected 20 core lesion brain regions. In order to prove the existence of this law, we have also expanded the number of brain regions. Figure 3(a'), Figure 3(b') and Figure 3(c') are the result of adding 10 brain regions on the basis of Figure 3(a),

TABLE 3. The two-classification average accuracy of different classifier.

Method	HC vs. EMCI			HC vs. LMCI			HC vs. AD			EMCI vs. LMCI			LMCI vs. AD		
	ACC	SEN	SPEC	ACC	SEN	SPEC	ACC	SEN	SPEC	ACC	SEN	SPEC	ACC	SEN	SPEC
RF	76.5%	75.0%	77.8%	76.5%	77.8%	75.0%	83.3%	100%	75.0%	73.3%	75.0%	71.4%	75.0%	66.7%	83.3%
SVM	86.7%	83.3%	88.9%	90.0%	90.0%	90.0%	93.3%	100%	88.9%	85.0%	83.3%	87.5%	86.7%	100%	75.0%
LR	81.3%	62.5%	100%	85.4%	95.8%	75.0%	87.5%	75.0%	100%	83.3%	100%	66.7%	83.3%	91.7%	75.0%
Ours	**91.7%**	87.5%	95.8%	**93.7%**	100%	87.5%	**95.8%**	91.7%	100%	**89.6%**	91.7%	87.5%	**91.7%**	87.5%	95.8%

TABLE 4. Comparison of classification accuracy for recent studies.

Authors	Target	Method	ACC	SEN	SPEC
Forouzannezhad et al.[20]	HCvsEMCI	DNN	84.0%	83.2%	84.4%
	HCvsLMCI		84.1%	80.4%	87.6%
	HCvsAD		96.8%	94.1%	98.2%
	EMCIvsLMCI		69.5%	80.6%	60.5%
	LMCIvsAD		80.2%	86.8%	71.9%
Zhang et al.[21]	HCvsEMCI	Spherical Sparse Coding	88.0%	82.0%	100%
	HCvsLMCI		94.0%	100%	91.0%
	HCvsAD		96.0%	91.0%	100%
	EMCIvsLMCI		84.0%	81.0%	100%
	LMCIvsAD		93.0%	89.0%	100%
Mehmood et al.[22]	HCvsEMCI	Layer-wise Transfer Learning	87.0%	86.6%	86.6%
	HCvsLMCI		89.1%	89.2%	88.9%
	HCvsAD		98.7%	98.2%	99.1%
	EMCIvsLMCI		81.1%	80.6%	81.5%
	LMCIvsAD		82.1%	81.4%	82.4%
Yang et al.[23]	HCvsEMCI	Fused Sparse Network	82.8%	69.7%	-
	HCvsLMCI		87.2%	75.6%	-
	EMCIvsLMCI		80.9%	71.1%	-
Ours	HCvsEMCI	SWLR	**91.7%**	87.5%	95.8%
	HCvsLMCI		93.7%	100%	87.5%
	HCvsAD		95.8%	91.7%	100%
	EMCIvsLMCI		**89.6%**	91.7%	87.5%
	LMCIvsAD		91.7%	87.5%	95.8%

Figure 3(b) and Figure 3(c). In Table 5, we show the five most informative features of each binary classification.

IV. DISCUSSIONS

The experimental results according to Table 3 and Table 4 show that our proposed idea of subclass weighting is effective and meaningful. By local weighting for subclasses, the coefficient values of some features can be modified in subclasses on the basis of the coefficient matrix constructed by LR, which can effectively reduce the interference of individual differences and improve the generalization ability of the model. In addition, according to Figure 3(a)-3(b), we also found that the distribution of core brain regions in different stages is also different, and the change trajectory of core brain regions on the two-dimensional image generally has a trend of continuous migration in the counterclockwise direction during the process of disease progression. This trend persisted even after we added 10 brain regions, as shown in Figures 3(a')-3(c'). Specifically, according to Figure 3(a), it can be seen that in the HC-EMCI stage, the core brain regions are mainly concentrated in the right half of the region, and a few parts appear in the lower half, which just shows that the core brain area of EMCI-LMCI stage will migrate downward. Figure 3(c) shows that the core brain area is mainly concentrated in the left half of the LMCI-AD stage. In addition, we compared our findings with existing studies, which we will describe in terms of microscopic and macroscopic.

TABLE 5. The most informative features of each binary classification.

Classfication	Feature	Hemisphere	Area
HC vs. EMCI	3337	L-97	i6-8
	2173	L-13	V3A
	1535	L-95	LIPd
	3249	L-9	3b
	1482	L-42	7AL
HC vs. LMCI	1781	R-161	31pd
	3492	R-72	10d
	3504	R-84	46
	1685	R-65	10r
	1644	R-24	A1
HC vs. AD	2233	L-73	8C
	1690	R-70	8BL
	1795	R-175	A4
	1726	R-106	PoI2
	1510	L-70	8BL
EMCI vs. LMCI	1663	R-43	SCEF
	1393	R-133	TE1p
	1644	R-24	A1
	1345	R-85	a9-46v
	1702	R-82	IFSa
LMCI vs. AD	1393	R-133	TE1p
	2151	R-171	p47r
	1976	L-176	STSva
	675	R-135	TF
	1422	R-162	31a

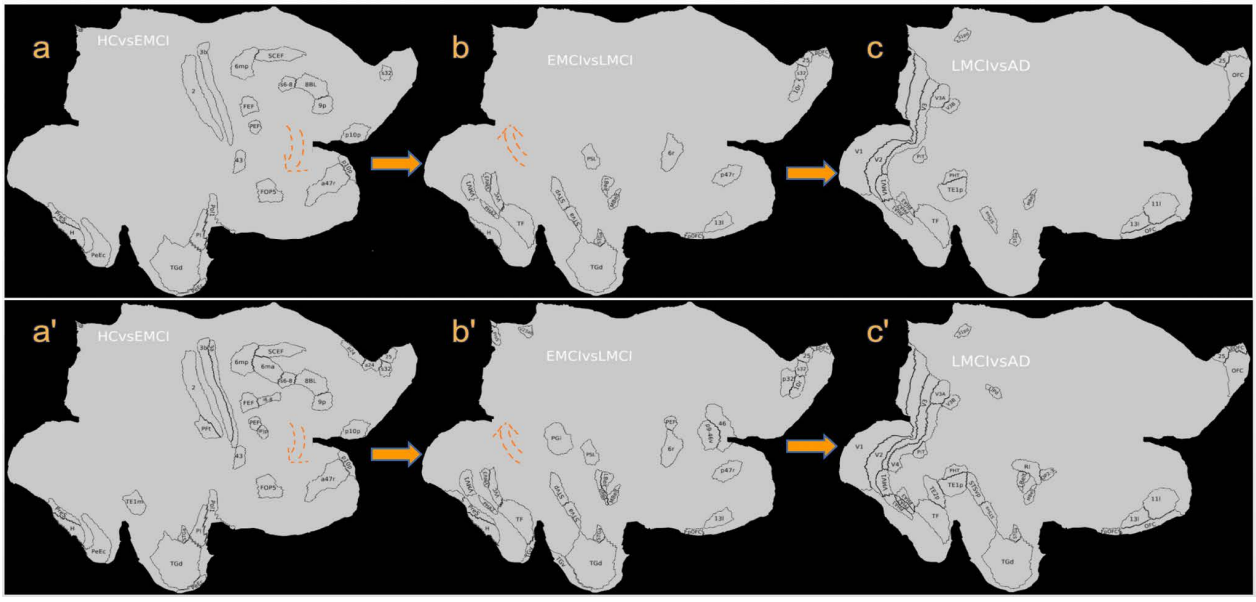

FIGURE 3. This picture describes the changes in the brain areas of the core deterioration at different stages, a–c describe the distribution of the first 20 core brain regions, and a'–c' are the result of adding 10 brain regions on the basis of a–c.

A. MACRO ASPECT

1) HC-EMCI STAGE

According to Figure 3(a) and Figure 4, it can be seen that the significant deterioration areas of HC-EMCI mainly involve sensor/motor, auditory and task negative. With regard to auditory, Swords *et al.* [24] pointed out that despite extensive brain atrophy in AD, specific structures seems to be at greater risk than other structures in prodromal stages of

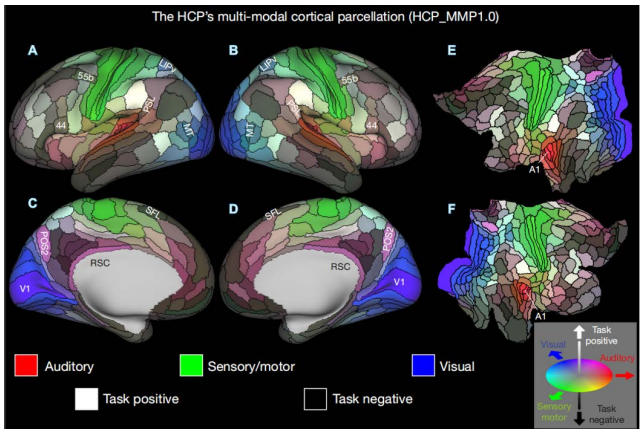

FIGURE 4. **This figure describes the functions of each region of the human brain, A-D are three dimensional drawing, E-F are two dimensional drawing, F stands for the right brain. The figure introduced by (Glasser MF, Coalson TS *et al.* 2016).**

disease, especially in the central auditory structure. In terms of sensory/motor, some longitudinal studies [25]–[29] show that a considerable number of patients have changes in sensory and motor systems in prodromal stages of AD. The changes of smell, hearing and even walking speed may precede the onset of cognitive impairment and dementia for 5 to 15 years, which is a strong risk factor for AD. Task negative, also known as default mode network, is composed of discrete, bilateral and symmetrical cortical regions, which are located in the medial and lateral parietal lobe, medial prefrontal lobe, medial and lateral temporal lobe cortex of human, non-human primates, cats and rodents. DMN will be less active when participating in cognitive tasks and more active at rest. In recent years, DMN has attracted extensive attention as a potential biomarker of AD [30], [31]. Some neuroimaging studies have shown that there are overlapping parts between amyloid plaque deposition area and DMN area [32]. In AD and MCI, the functional connection of DMN is destroyed [33]–[35]. Since the functional connectivity in DMN has been noted to have an impact on episodic memory, the destruction of DMN connectivity may be a potential cause of early memory loss in AD patients [36].

2) EMCI-LMCI STAGE

According to Figure 3(b) and Figure 4, it can be seen that the significant deterioration area of EMCI-LMCI mainly involves two aspects of Auditory and Task negative, which are similar to those involved in HC-EMCI, so I will not repeat them here.

3) LMCI-AD STAGE

According to Figure 3(c) and Figure 4, it can be seen that the significant deterioration area of LMCI-AD mainly involves Task negative and Visual. Visual is an aspect that is significantly different from the previous two stages, so it is of great research value. Lavallee *et al.* [37] pointed out that AD patients have deficits in higher-level visual processes, more specifically in perceiving individual faces, a function that relies on global representations of upright facial stimuli. These deficits, combined with their memory impairment, can lead to difficulty recognizing familiar people. Hinton *et al.* [38] showed extensive optic axonal degeneration in AD patients. Using different staining and morphological methods, Albers *et al.* [39] integrated the literature on ad sensory system disorders and found that ad related pathology was found in both cortical and subcortical areas related to visual function in addition to the eye itself.

B. MICRO ASPECT

As HCPMMP is the most granularly brain zoning method at present, there is a lack of corresponding research on some new brain regions proposed by HCP. We can only select some brain regions for further analysis according to the existing literature and the weight coefficient of brain regions. Another point to be explained is that there are few studies on EMCI and LMCI, we can only prove that the brain regions involved in EMCI and LMCI stage act on MCI stage.

1) HC-EMCI STAGE

S6-8, 8BL and 9p belong to dorsal prefrontal cortex (DLPFC) Syed *et al.* [40] found that the bilateral activation of DLPFC in MCI group was significantly higher than that in HC group. Hyperactivity of DLPFC has also been found previously and is considered to reflect the compensatory mechanism of several behavioral defects. S6-8, also known as frontal cortex (FC), is located in the frontal cortex. Ansari and Scheff [41] studied the oxidative stress of FC after death in 8 samples with mild cognitive impairment. 10 subjects without cognitive impairment matched with these cases were used as controls. It was found that the oxidative stress of FC tissue in MCI patients was significantly higher than that in healthy controls. PeEc corresponds to BA35 and BA36 in the traditional division, while h is the hippocampus, which belongs to the medical temporal cortex (MTL), Xie *et al.* [42] studied the subregions of the medical temporal cortex (MTL). His study showed that the longitudinal atrophy rate of all MTL subregions of early prodromal AD was significantly higher than that of the healthy control group, and longitudinal changes in BA35 showed the strongest statistical significance in distinguishing AD patients with early prodromal symptoms from amyloid-β negative controls. Furthermore, neuropathological and structural MRI studies have shown that MTL is the earliest affected brain region in AD [43]. 3b belongs to the primary somatosensory cortex (S1), which contains two regions 3b and 3a. 3b is related to human somatic sensation. Some studies in recent years have begun to show that sensorimotor dysfunction occurs earlier than previously thought. Suva *et al.* [44] found that once senile plaques were found in other cortical related areas, senile plaques were found in sensorimotor areas. Initially, only the hippocampus showed isolated plaques. Stephen *et al.* [45] found that in the first three peaks of primary somatosensory source response, MCI patients showed

larger amplitude responses than HC and AD groups (P\0.03). Other relationships between neuropsychological measures and SI amplitudes were also determined. Amplitudes of contralateral secondary somatosensory sources did not differ significantly across diagnostic categories. These results suggest that the somatosensory cortex is affected early in AD progression and may have implications for behavioral and functional measures. TGd is one of two brain regions that form temporal polar cortex (TPC), and TPC has been shown to be one of the earliest causes of AD disease [46]–[48].

2) EMCI-LMCI STAGE

Many brain regions involved in this stage have been discussed in the HC-EMCI section, and we will focus on selecting brain regions not mentioned above for analysis. EMCI-LMCI and HC-EMCI stage have two notable differences. In EMCI-LMCI stage, Ventral Stream Visual Cortex and Auditory Cortex have a significant impact on disease development. Auditory Cortex contains LBelt, MBelt, STVa, STVp, STGa in the diagram. Recent studies have shown that both peripheral and central auditory system dysfunction occur in the prodromal stages of Alzheimer's disease (AD). Rahman *et al.* [49] performed a central auditory processing test in MCI patients in addition to using pure tone audiometry (PTA) immittance, selective auditory attention test (PPS), and pitch pattern test (GFW). They found that MCI patients scored significantly lower than controls on the selective auditory attention test (SAAT), dichotic digitstest (DDT) left ear, pitch pattern sequence (PPS) and Goldman-Fristoe-Woodcock (GFW) tests. Ventral Stream Visual Cortex contains the VMV1, VMV3, and VVC brain regions in Figure 3(b). Data show that cortical visual processing is divided into dorsal and ventral streams, with the ventral stream processing object recognition of visual or ''what'' features [50], [51]. Graewe *et al.* [52] added to previous fMRI studies by exploring temporal and parietal mechanisms in healthy aging and MCI using a related cognitive task (perception of motor-defined facial stimuli). They found that during structure-from-motion face perception in MCI, there is an overemphasis on low-level cognition at the expense of overall processing, which are aberrant activation patterns in the fusiform face area (FFA)/occipital face area (OFA). Furthermore, MCI is characterized by alterations in the dorsal-ventral integration area and attention-related networks. Although previous studies have highlighted visual dorsal flow dysfunction in MCI they found that the FFA/OFA activity pattern in the visual ventral region is a highly accurate biomarker of MCI.

3) LMCI-AD STAGE

The biggest difference between this stage and EMCI-LMCI is that there are a large number of cortices related to vision. V1 belongs to Primary Visual Cortex, V2 and V3 belong to Early Visual Cortex, VMV1 belongs to Ventral Stream Visual Cortex, and V3A and V3B belong to Dorsal Stream Visual Cortex. Past studies have shown that cholinergic deficits in the primary visual cortex may underlie some abnormalities in visual processing and overall cognitive performance in Alzheimer's disease (AD). Ikonomovic *et al.* [53] assessed (choline acetyltransferase) ChAT and (acetylcholinesterase) AChE activity and ((nerve growth factor) NGF protein levels in the primary visual cortex of subjects without cognitive impairment (NCI), mild cognitive impairment (MCI) and AD, and the results showed that Decreased ChAT activity was found in primary visual cortex in to moderate AD but not in MCI, a finding that clearly points to differences in primary visual cortex at MCI and AD stages, consistent with our findings. There are few related studies on Early Visual Cortex, but V2, V3 are important components of the dorsal and ventral visual pathways. The Dorsal Stream Visual Cortex associated with V3A, V3B is mainly related to motor information, and Yamasaki *et al.* [54] studied the differences in dorsal flow changes between MCI and AD patients and healthy controls. They recorded (event-related potentials) ERPs of AD and MCI patients and healthy controls in response to optic flow (OF) and horizontal (HO) motor stimuli. Movement-related N170 (V5/middle temporal (MT) origin) and OF-specific P200 (v-d origin) were major components in all groups. Compared with healthy controls, MCI patients had prolonged P200 latency to both stimuli, but not N170 latency. In contrast, AD patients had significantly longer latencies to both stimuli N170 and P200 compared to the other groups, a finding that demonstrates that there are also differences in dorsal flow changes between AD and MCI patients.

V. CONCLUSION

In this paper, we proposed a new subclass weighting algorithm based on logistic regression, namely the SWLR algorithm. Specifically, K-means++ clustering samples is performed, and several samples with similar Euclidean distances are regarded as a subclass. Establish a subclass weight for each subclass. The predicted label of the final sample is jointly determined by the subclass weight and the global weight. In order to prevent over fitting and improve the problem that the dimension of the feature set is too high, we adopt L2 regularization for both U and V in the loss function. In order to prove the effectiveness of the algorithm, we did five sets of comparative experiments, namely HC vs. EMCI, HC vs. LMCI, EMCI vs. LMCI, LMCI vs. AD, and HC vs. AD. Experiments show that the SWLR algorithm has decent performance. In addition, we conducted the follow-up analysis of the coefficient matrix U, selected the features with the highest weight coefficients in each stage, and then located the corresponding brain regions in the toolbox provided by HCPMMP. We found that during the development of the disease from HC to AD, there is a law in the distribution of the core brain region, which generally migrates counterclockwise. Then, we compare our findings with the existing research from both macro and micro aspects, and the results show that our findings are consistent with the existing research. It is worth mentioning that, in view of the current

research literature on EMCI and LMCI is less, our research can be said to be enlightening.

REFERENCES

[1] A. Kingston, A. Comas-Herrera, and C. Jagger, "Forecasting the care needs of the older population in England over the next 20 years: Estimates from the population ageing and care simulation (PACSim) modelling study," *Lancet Public Health*, vol. 3, no. 9, pp. e447–e455, Sep. 2018.

[2] C. Patterson, "The state of the art of dementia research: New frontiers," Alzheimer's Disease Int. (ADI), London, U.K., World Alzheimer's Rep. 2018, 2018.

[3] R. Roberts and D. S. Knopman, "Classification and epidemiology of MCI," *Clinics Geriatric Med.*, vol. 29, no. 4, pp. 752–753, Nov. 2013.

[4] P. S. Aisen, R. C. Petersen, M. C. Donohue, A. Gamst, R. Raman, R. G. Thomas, S. Walter, J. Q. Trojanowski, L. M. Shaw, L. A. Beckett, C. R. Jack, W. Jagust, A. W. Toga, A. J. Saykin, J. C. Morris, R. C. Green, M. W. Weiner, and I. Alzheimer's Disease Neuroimaging, "Clinical core of the Alzheimer's disease neuroimaging initiative: Progress and plans," *Alzheimer's Dementia*, vol. 6, no. 3, pp. 239–246, May 2010.

[5] E. M. Reiman and W. J. Jagust, "Brain imaging in the study of Alzheimer's disease," *NeuroImage*, vol. 61, no. 2, pp. 505–516, Jun. 2012.

[6] V. Betti, S. Della Penna, F. de Pasquale, D. Mantini, L. Marzetti, G. L. Romani, and M. Corbetta, "Natural scenes viewing alters the dynamics of functional connectivity in the human brain," *Neuron*, vol. 79, no. 4, pp. 782–797, Aug. 2013.

[7] M. D. Fox, A. Z. Snyder, J. L. Vincent, and M. E. Raichle, "Intrinsic fluctuations within cortical systems account for intertrial variability in human behavior," *Neuron*, vol. 56, no. 1, pp. 84–171, Oct. 2007.

[8] J. C. Gore, "Principles and practice of functional MRI of the human brain," *J. Clin. Invest.*, vol. 112, no. 1, pp. 4–9, 2003.

[9] K. Arfanakis, D. Cordes, V. M. Haughton, C. H. Moritz, M. A. Quigley, and M. E. Meyerand, "Combining independent component analysis and correlation analysis to probe interregional connectivity in fMRI task activation datasets," *Magn. Reson. Imag.*, vol. 18, no. 8, pp. 921–930, Oct. 2000.

[10] D. A. Fair, B. L. Schlaggar, A. L. Cohen, F. M. Miezin, N. U. Dosenbach, K. K. Wenger, M. D. Fox, A. Z. Snyder, M. E. Raichle, and S. E. Petersen, "A method for using blocked and event-related fMRI data to study 'resting state' functional connectivity," *NeuroImage*, vol. 35, no. 1, pp. 396–405, Mar. 2007.

[11] M. D. Fox, A. Z. Snyder, J. M. Zacks, and M. E. Raichle, "Coherent spontaneous activity accounts for trial-to-trial variability in human evoked brain responses," *Nature Neurosci.*, vol. 9, no. 1, pp. 5–23, Jan. 2006.

[12] S. M. Smith, P. T. Fox, K. L. Miller, D. C. Glahn, P. M. Fox, C. E. Mackay, N. Filippini, K. E. Watkins, R. Toro, A. R. Laird, and C. F. Beckmann, "Correspondence of the brain's functional architecture during activation and rest," *Proc. Nat. Acad. Sci. USA*, vol. 106, no. 31, pp. 13040–13045, 2009.

[13] M. F. Glasser, T. S. Coalson, E. C. Robinson, C. D. Hacker, J. Harwell, E. Yacoub, K. Ugurbil, J. Andersson, C. F. Beckmann, M. Jenkinson, S. M. Smith, and D. C. Van Essen, "A multi-modal parcellation of human cerebral cortex," *Nature*, vol. 536, no. 7615, pp. 171–178, Aug. 2016.

[14] J. Sheng, B. Wang, Q. Zhang, Q. Liu, Y. Ma, W. Liu, M. Shao, and B. Chen, "A novel joint HCPMMP method for automatically classifying Alzheimer's and different stage MCI patients," *Behavioural Brain Res.*, vol. 365, pp. 210–221, Jun. 2019.

[15] G. Gosztolya, V. Vincze, L. Tóth, M. Pákáski, J. Kálmán, and I. Hoffmann, "Identifying mild cognitive impairment and mild Alzheimer's disease based on spontaneous speech using ASR and linguistic features," *Comput. Speech Lang.*, vol. 53, pp. 181–197, Jan. 2019.

[16] J. Peng, X. Zhu, Y. Wang, L. An, and D. Shen, "Structured sparsity regularized multiple kernel learning for Alzheimer's disease diagnosis," *Pattern Recognit.*, vol. 88, pp. 370–382, Apr. 2019.

[17] S. Wang, H. Wang, A. C. Cheung, Y. Shen, and M. Gan, "Ensemble of 3D densely connected convolutional network for diagnosis of mild cognitive impairment and Alzheimer's disease," in *Deep Learning Applications*, M. A. Wani, M. Kantardzic, and M. Sayed-Mouchaweh, Eds. Singapore: Springer, 2020, pp. 53–73.

[18] S. Spasov, L. Passamonti, A. Duggento, P. Lió, and N. Toschi, "A parameter-efficient deep learning approach to predict conversion from mild cognitive impairment to Alzheimer's disease," *NeuroImage*, vol. 189, pp. 276–287, Apr. 2019.

[19] A. Khazaee, A. Ebrahimzadeh, and A. Babajani-Feremi, "Application of advanced machine learning methods on resting-state fMRI network for identification of mild cognitive impairment and Alzheimer's disease," *Brain Imag. Behav.*, vol. 10, no. 3, pp. 799–817, Sep. 2016.

[20] P. Forouzannezhad, A. Abbaspour, C. Li, M. Cabrerizo, and M. Adjouadi, "A deep neural network approach for early diagnosis of mild cognitive impairment using multiple features," in *Proc. 17th IEEE Int. Conf. Mach. Learn. Appl. (ICMLA)*, Dec. 2018, pp. 1341–1346.

[21] J. Zhang, Y. Fan, Q. Li, P. M. Thompson, J. Ye, and Y. Wang, "Empowering cortical thickness measures in clinical diagnosis of Alzheimer's disease with spherical sparse coding," in *Proc. IEEE 14th Int. Symp. Biomed. Imag. (ISBI)*, Apr. 2017, pp. 446–450.

[22] A. Mehmood, S. Yang, Z. Feng, M. Wang, A. S. Ahmad, R. Khan, M. Maqsood, and M. Yaqub, "A transfer learning approach for early diagnosis of Alzheimer's disease on MRI images," *Neuroscience*, vol. 460, pp. 43–52, Apr. 2021.

[23] P. Yang, F. Zhou, D. Ni, Y. Xu, S. Chen, T. Wang, and B. Lei, "Fused sparse network learning for longitudinal analysis of mild cognitive impairment," *IEEE Trans. Cybern.*, vol. 51, no. 1, pp. 233–246, Jan. 2021.

[24] G. M. Swords, L. T. Nguyen, R. A. Mudar, and D. A. Llano, "Auditory system dysfunction in Alzheimer disease and its prodromal states: A review," *Ageing Res. Rev.*, vol. 44, pp. 49–59, Jul. 2018.

[25] D. P. Devanand, X. Liu, M. H. Tabert, G. Pradhaban, K. Cuasay, K. Bell, M. J. de Leon, R. L. Doty, Y. Stern, and G. H. Pelton, "Combining early markers strongly predicts conversion from mild cognitive impairment to Alzheimer's disease," *Biol. Psychiatry*, vol. 64, no. 10, pp. 871–879, Nov. 2008.

[26] G. A. Gates, M. L. Anderson, M. P. Feeney, S. M. Mccurry, and E. B. Larson, "Central auditory dysfunction in older persons with memory impairment or Alzheimer dementia," *Arch. Otolaryngol. Head Neck Surg.*, vol. 134, no. 7, pp. 771–777, 2008.

[27] F. R. Lin, E. J. Metter, R. J. O'Brien, S. M. Resnick, A. B. Zonderman, and L. Ferrucci, "Hearing loss and incident dementia," *Arch. Neurol.*, vol. 68, no. 2, pp. 214–220, Feb. 2011.

[28] R. S. Wilson, J. A. Schneider, J. L. Bienias, D. A. Evans, and D. A. Bennett, "Parkinsonianlike signs and risk of incident Alzheimer disease in older persons," *Arch. Neurol.*, vol. 60, no. 4, pp. 539–544, 2003.

[29] J. Verghese, C. Wang, R. B. Lipton, R. Holtzer, and X. Xue, "Quantitative gait dysfunction and risk of cognitive decline and dementia," *J. Neurol., Neurosurgery Psychiatry*, vol. 78, no. 9, pp. 929–935, Sep. 2007.

[30] M. L. Balthazar, B. M. de Campos, A. R. Franco, B. P. Damasceno, and F. Cendes, "Whole cortical and default mode network mean functional connectivity as potential biomarkers for mild Alzheimer's disease," *Psychiatry Res., Neuroimaging*, vol. 221, no. 1, pp. 37–42, Jan. 2014.

[31] W. Koch, S. Teipel, S. Mueller, J. Benninghoff, M. Wagner, A. L. Bokde, H. Hampel, U. Coates, M. Reiser, and T. Meindl, "Diagnostic power of default mode network resting state fMRI in the detection of Alzheimer's disease," *Neurobiol. Aging*, vol. 33, no. 3, pp. 466-478, Mar. 2012.

[32] W. E. Klunk, H. Engler, A. Nordberg, Y. Wang, G. Blomqvist, D. P. Holt, M. Bergström, I. Savitcheva, G. F. Huang, S. J. Estrada, and T. C. N. Society, "Imaging brain amyloid in Alzheimer's disease with Pittsburgh Compound-B," *Ann. Neurol., Off. J. Amer. Neurol. Assoc. Child Neurol. Soc.*, vol. 55, no. 3, pp. 306–319, 2004.

[33] F. Bai, D. R. Watson, H. Yu, Y. Shi, Y. Yuan, and Z. Zhang, "Abnormal resting-state functional connectivity of posterior cingulate cortex in amnestic type mild cognitive impairment," *Brain Res.*, vol. 1302, pp. 167–174, Dec. 2009.

[34] M. D. Greicius, G. Srivastava, A. L. Reiss, and V. Menon, "Default-mode network activity distinguishes Alzheimer's disease from healthy aging: Evidence from functional MRI," *Proc. Nat. Acad. Sci. USA*, vol. 101, no. 13, pp. 4637–4642, 2004.

[35] S. A. Rombouts, F. Barkhof, R. Goekoop, C. J. Stam, and P. Scheltens, "Altered resting state networks in mild cognitive impairment and mild Alzheimer's disease: An fMRI study," *Hum. Brain Mapping*, vol. 26, no. 4, pp. 231–239, Dec. 2005.

[36] W. S. Sohn, K. Yoo, D. L. Na, Y. J. A. D. Jeong, and A. Disorders, "Progressive changes in hippocampal resting-state connectivity across cognitive impairment: A cross-sectional study from normal to Alzheimer disease," *Alzheimer Disease Associated Disorders*, vol. 28, no. 3, pp. 239–246, 2014.

[37] M. M. Lavallee, D. Gandini, I. Rouleau, G. T. Vallet, M. Joannette, M. J. Kergoat, T. Busigny, B. Rossion, and S. Joubert, "A qualitative impairment in face perception in Alzheimer's disease: Evidence from a reduced face inversion effect," *J. Alzheimer's Disease*, vol. 51, no. 4, pp. 1225–1236, 2016.

[38] D. R. Hinton, A. A. Sadun, J. C. Blanks, and C. A. Miller, "Optic-nerve degeneration in Alzheimer's disease," *New England J. Med.*, vol. 315, no. 8, pp. 485–487, 1986.

[39] M. W. Albers *et al.*, "At the interface of sensory and motor dysfunctions and Alzheimer's disease," *Alzheimer's Dementia, J. Alzheimer's Assoc.*, vol. 11, no. 1, pp. 70–98, 2015.
[40] A. Syed, R. Armstrong, and C. Smith, "A quantitative analysis of optic nerve axons in elderly control subjects and patients with Alzheimer's disease," *Folia Neuropathol.*, vol. 43, pp. 1–6, Jan. 2005.
[41] M. A. Ansari and S. W. Scheff, "Oxidative stress in the progression of Alzheimer disease in the frontal cortex," *J. Neuropathol. Exp. Neurol.*, vol. 69, no. 2, pp. 67–155, Feb. 2010.
[42] L. Xie, L. E. M. Wisse, S. R. Das, N. Vergnet, M. Dong, R. Ittyerah, R. de Flores, P. A. Yushkevich, and D. A. Wolk, "Longitudinal atrophy in early Braak regions in preclinical Alzheimer's disease," *Hum. Brain Mapping*, vol. 41, no. 16, pp. 4704–4717, Nov. 2020.
[43] L. Mosconi, "Brain glucose metabolism in the early and specific diagnosis of Alzheimer's disease. FDG-PET studies in MCI and AD," *Eur. J. Nucl. Med. Mol. Imag.*, vol. 32, no. 4, pp. 486–510, Apr. 2005.
[44] D. Suva, I. Favre, R. Kraftsik, M. Esteban, A. Lobrinus, and J. Miklossy, "Primary motor cortex involvement in Alzheimer disease," *J. Neuropathol. Exp. Neurol.*, vol. 58, no. 11, pp. 1125–1134, Nov. 1999.
[45] J. M. Stephen, R. Montano, C. H. Donahue, J. C. Adair, J. Knoefel, C. Qualls, B. Hart, D. Ranken, and C. J. Aine, "Somatosensory responses in normal aging, mild cognitive impairment, and Alzheimer's disease," *J. Neural Transmiss.*, vol. 117, no. 2, pp. 217–225, Feb. 2010.
[46] S. L. Ding, G. W. Van Hoesen, M. D. Cassell, and A. Poremba, "Parcellation of human temporal polar cortex: A combined analysis of multiple cytoarchitectonic, chemoarchitectonic, and pathological markers," *J. Comparative Neurol.*, vol. 514, no. 6, pp. 595–623, Jun. 2009.
[47] M. Hoistad and H. Barbas, "Sequence of information processing for emotions through pathways linking temporal and insular cortices with the amygdala," *NeuroImage*, vol. 40, no. 3, pp. 1016–1033, Apr. 2008.
[48] S. E. Arnold, B. T. Hyman, J. Flory, A. R. Damasio, and G. W. Van Hoesen, "The topographical and neuroanatomical distribution of neurofibrillary tangles and neuritic plaques in the cerebral cortex of patients with Alzheimer's disease," *Cerebral Cortex*, vol. 1, no. 1, pp. 103–116, Jan. 1991.
[49] T. T. Rahman, S. T. Mohamed, M. H. Albanouby, and H. F. Bekhet, "Central auditory processing in elderly with mild cognitive impairment," *Geriatrics Gerontol. Int.*, vol. 11, no. 3, pp. 304–308, Jul. 2011.
[50] R. E. Weller, "Two cortical visual systems in old world and new world primates," in *Progress in Brain Research*, vol. 75. Jan. 1988, ch. 27, pp. 293–306.
[51] D. J. Kravitz, K. S. Saleem, C. I. Baker, and M. Mishkin, "A new neural framework for visuospatial processing," *Nature Rev. Neurosci.*, vol. 12, no. 4, pp. 217–230, Apr. 2011.
[52] B. Graewe, R. Lemos, C. Ferreira, I. Santana, R. Farivar, P. De Weerd, and M. Castelo-Branco, "Impaired processing of 3D motion-defined faces in mild cognitive impairment and healthy aging: An fMRI study," *Cerebral Cortex*, vol. 23, no. 10, pp. 2489–2499, Oct. 2013.
[53] M. D. Ikonomovic, E. J. Mufson, J. Wuu, D. A. Bennett, and S. T. DeKosky, "Reduction of choline acetyltransferase activity in primary visual cortex in mild to moderate Alzheimer's disease," *Arch. Neurol.*, vol. 62, no. 3, pp. 425–430, 2005.
[54] T. Yamasaki, Y. Goto, Y. Ohyagi, A. Monji, S. Munetsuna, M. Minohara, K. Minohara, J.-I. Kira, S. Kanba, and S. Tobimatsu, "A deficit of dorsal stream function in patients with mild cognitive impairment and Alzheimer's disease," in *Proc. Int. Conf. Complex Med. Eng. (ICME)*, 2012, pp. 28–31.

JINHUA SHENG (Senior Member, IEEE) received the Ph.D. degree in nuclear electronics from the University of Science and Technology of China, in 1997.

From April 2005 to December 2008, he was a Postdoctoral Research Associate with the University of Wisconsin–Milwaukee, Milwaukee, WI, USA. He is currently a Distinguished Professor with the College of Computer Science and Technology, Hangzhou Dianzi University; the Deputy Director of Institute of "Cognitive and Intelligent Computing," Hangzhou Dianzi University; and the Director of the Key Laboratory of "Intelligent Image Analysis for Sensory and Cognitive Health," Ministry of Industry and Information Technology of China, Hangzhou, China. He had 16 years of experience as a Postdoctoral Research Associate, a Research Scientist, a Research Associate, a Research Fellow, and a Faculty Member at the prominent institutions of the USA. As an Expert in image processing, medical imaging science and neuroscience, he has contributed a lot in his area of specialization with over 70 research papers in some peer-reviewed journals and important international conferences, and been granted one U.S. patent, and seven Chinese patents. While in U.S., he worked on the National Institutes of Health (NIH) and the National Science Foundation (NSF) research grants with over U.S. $6 000 000. As a Principal Investigator, he has been working on National Natural Science Foundation of China and other grants with over ¥2 000 000 RMB, since 2018. He is an active reviewer for many peer-reviewed journals and some important international conferences with over 100 research papers. His research works have been reported in some professional media, such as science daily. He a fellow of IET, in 2022. He served as the chief editor for one journal in China and serves as an Associate Editor for IEEE Access and an Editorial Board Member for *Scientific Reports*.

SHUAI WU received the bachelor's degree from Zhejiang A&F University, China, in 2020. He is currently pursuing the master's degree in computer science with Hangzhou Dianzi University, China. His main research interests include neuroscience, Alzheimer's disease, and machine learning.

QIAO ZHANG received the M.D. degree from Bengbu Medical University, China, in 1988. From May 2006 to June 2009, she worked as a Visiting Scholar at the Northwestern University Feinberg School of Medicine, USA. Currently, she is a Full Professor with the Peking Union Medical College Hospital; and the Institute of Geriatric Medicine, Chinese Academy of Medical Sciences. She has contributed a lot in clinical medicine as a Researcher and a Clinical Expert. She has published more than 40 research articles.

ZHONGJIN LI received the Ph.D. degree from the Software Institute, Nanjing University, Nanjing, China, in 2017. He is currently an Associate Professor with the College of Computer Science and Technology, Hangzhou Dianzi University, Hangzhou, China. His research interests include cloud workflow scheduling, mobile edge computing, video semantic segmentation, and machine learning.

HE HUANG received the B.S. degree from Hangzhou Dianzi University, China, in 2018, where he is currently pursuing the M.S. degree. His main research interests include Alzheimer's disease, neuroscience, and machine learning.